

Broken Symmetries in Quasi-2D Charged Systems via Dielectric Confinement

Xuanzhao Gao^{1,2,*} and Zecheng Gan^{1,3,†}

¹*Thrust of Advanced Materials, The Hong Kong University of Science and Technology (Guangzhou), Guangdong, China*

²*Department of Physics, The Hong Kong University of Science and Technology, Hong Kong SAR, China*

³*Department of Mathematics, The Hong Kong University of Science and Technology, Hong Kong SAR, China*

(Dated: July 12, 2022)

Quasi-2D charged systems are attracting much attention because of their potential in future nanodevices. The confined geometry gives rise to new collective phases, but also brings great challenges for computational studies. We derive an analytic, fast convergent lattice summation formula for the simulation of charged particles under dielectric confinement, and demonstrate that spontaneous symmetry breaking (SSB) can be triggered solely via the substrate permittivity. Interestingly, dielectric contrast can even determine the degree of SSB in longitudinal and transverse dimensions, forming charge-separated interfacial liquids and correlated-clusters. The novel broken symmetry mechanism may shed light in understanding a variety of quasi-2D systems.

Among various long-range systems, quasi-2D charged systems are of great importance, and have caught much attention recently because of their huge potential in future nanodevices and advanced materials. Typically, quasi-2D systems are with nano-sized longitudinal thickness in z direction (usually by confinement), bulk-like and modeled as periodic in transverse xy directions [1]. Rich new collective behaviors arise in such systems, to name a few, polyelectrolyte adsorption and structure [2, 3], ion transport and selectivity [4, 5].

Nevertheless, in terms of the spontaneous symmetry breaking (SSB) phenomena, much existing study focuses on purely 2D and 3D systems [6–8], far less is known about quasi-2D. For bulk electrolytes or neutral plasma, it is well-known that the Coulomb potential can be dynamically screened by surrounding countercharges, leading to effectively short-range interacting particle systems [9]. The situation becomes very different in quasi-2D charged systems: their reduced symmetry (i.e., the nano-sized confinement) weakens the electrostatic screening, and correlation effect can become much more important. Clearly, this is quasi-2D specific, where simplified 2D description would fail. Yet, to the best of our knowledge, no SSB phenomena have been reported in suspension of charge- and size-symmetric, overall-neutral particle systems under dielectric confinement, without any external fields.

Another important effect associated with quasi-2D charged systems concerns the permittivity, i.e., the *dielectric confinement effect*. Substrate materials for nanoscale confinement can range from dielectric to metallic, and nowadays, electromagnetic metamaterials, described by permittivities that can take negative values [10, 11]. For electrolytes/polymers near a *single* dielectric substrate, recently calculations have revealed that the dielectric surface effect can greatly deviate the systems from bulk behaviors, such as ion transport [12], polymer brush structure [3] and pattern formation in dipolar films [13]. Unfortunately, the addition of a second dielectric substrate to actually form dielectric confine-

ment in computer simulations is far from direct-forward: simulation techniques [14–25] have made great progress over the past decades, but proper treatment of the dielectric confinement effect with satisfactory accuracy and efficiency remains challenging.

In this letter, we develop a new lattice summation formula for the Green’s function in simulating charged particles under dielectric confinement, its spectral convergence allows us to efficiently calculate the polarization field. Through computer simulations of a prototypical charge- and size-symmetric binary mixture of particles described by the primitive model [26], we demonstrate that broken symmetries arise spontaneously due to the dielectric confinement effect alone. Moreover, we discover that the substrate permittivity can even qualitatively alter the degree of SSB in longitudinal and transverse dimensions, forming charge-separated interfacial liquids and correlated-clusters. Noteworthy is that all the SSB phenomena reported here actually require the presence of *two* dielectric substrates, we attribute this to the complicated multiply scattered polarization field due to the layered dielectric confinement structure.

The Green’s function $G(\mathbf{r}; \mathbf{r}')$ for a doubly-periodic, dielectric confined geometry is described by the Poisson’s equation,

$$-\nabla \cdot [\epsilon(\mathbf{r}) \nabla G(\mathbf{r}; \mathbf{r}')] = \sum_{\|\mathbf{m}\|=0}^{+\infty} \delta(\mathbf{r} - \mathbf{r}'_{\mathbf{m}}), \quad (1)$$

where $\mathbf{r}, \mathbf{r}' \in [0, L_x] \times [0, L_y] \times [0, L_z]$ are the target and source locations within the simulation box, $\mathbf{r}'_{\mathbf{m}} = \mathbf{r}' + m_x L_x \hat{\mathbf{x}} + m_y L_y \hat{\mathbf{y}}$ accounts for the periodic replicas along x and y directions, with $\mathbf{m} = (m_x, m_y)$ the 2D lattice vector, $m_x, m_y \in \mathbb{Z}$. Importantly, $\epsilon(\mathbf{r})$ is the material-specific, spatially varying dielectric constant, as is depicted in Fig. 1. Finally, we have the dielectric interface conditions, i.e., the continuity of $G(\mathbf{r}; \mathbf{r}')$ and $\epsilon(\mathbf{r}) \partial G(\mathbf{r}; \mathbf{r}') / \partial z$ across $z = 0$ and L_z , and the free-space boundary condition (FBC) as $z \rightarrow \pm\infty$. Note that for charges under dielectric confinement, proposing the

arXiv:2207.04687v1 [cond-mat.soft] 11 Jul 2022

proper FBC needs careful considerations so as to make it physically well-defined, which we will clarify later.

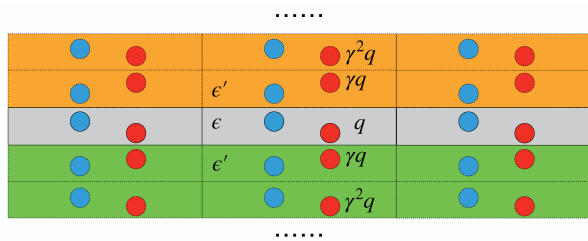


FIG. 1. Schematic depiction of a quasi-2D charged system, the dielectric confinement effect is illustrated from the Image Charge Method (ICM) view point. The grey region represents the solvent medium with dielectric permittivity ϵ , orange and green regions represent upper and lower substrate with dielectric permittivity ϵ' . Red and blue circles surrounded by solid lines are actual charged particles of the doubly-periodic system, while those surrounded by dotted lines are their images reflected by dielectric interfaces.

To gain insight in the role of dielectric confinement in quasi-2D systems, we start our discussion with the classic Image Charge Method (ICM). Consider a point charge q located in a medium with dielectric constant ϵ , and near a single planar substrate with dielectric constant ϵ' , the polarization potential can be equivalently expressed as the Coulomb potential generated by an image charge located with mirror-symmetry, and magnitude $q_{\text{img}} = \gamma q$. The dimensionless coefficient $\gamma = (\epsilon - \epsilon') / (\epsilon + \epsilon')$ quantifies the strength of polarization. Usually, $|\gamma| \leq 1$ for materials with positive permittivities, but the upper bound can be further lifted for metamaterials because of their stronger polarizability, characterized by negative permittivity values [27, 28]. Based on the ICM, the Green's function in Eq. (1) can be further constructed via a multiple reflection process, resulting in an infinite image charge series, which is also schematically illustrated in Fig. 1. Note that when $|\gamma| \leq 1$, the image reflection series is convergent; but when $|\gamma| > 1$, it will be *divergent* and thus the reflective ICM approach would fail. Due to this divergent difficulty, current simulation studies in the $|\gamma| > 1$ regime is still limited to a single dielectric substrate [13]. Our new approach overcomes this divergence issue via a proper renormalization strategy, which allows us to extensively explore the dielectric confinement effect in all possible γ regimes, especially the less explored scenario of metamaterial substrates.

The dielectric confinement effect turns out to be physically interesting even when only two charged particles are present. In Fig. 2, we plot the electrostatic force F_x between two likely charged particles as a function of their center-to-center distance Δx , with varying values of γ ranging from -10 to $+10$. The two particles are symmetric both in charge and size (same valence ν , diameter τ_0), placed at $\mathbf{r}_1 = (15\tau_0, 15\tau_0, \tau_0)$

and $\mathbf{r}_2 = (15\tau_0 + \Delta x, 15\tau_0, \tau_0)$ inside a box of size $30\tau_0 \times 30\tau_0 \times 2\tau_0$. The electrostatic energy of the two-particle system can be written as $U_{\text{elec}} = (\nu e_0)^2 G(\mathbf{r}_1, \mathbf{r}_2)$, with the Green's function G defined in Eq. (1) and the Bjerrum length $\ell_B = e_0^2 / (4\pi\epsilon k_B T)$ characterizing the electrostatic coupling strength of the solvent, with e_0 the elementary charge, k_B the Boltzmann constant, and T for temperature. The electrostatic force thus can be defined as $F_x = -\partial U_{\text{elec}} / \partial x$, a positive value of F_x indicates repulsion and negative represents attraction. Surprisingly, we observe from Fig. 2 a *continuous transition* from like-charge attraction (LCA) into repulsion and then even oscillatory interaction as γ increases from -10 to $+10$. This shows a clear dominance of the dielectric confinement effect over the bare Coulomb repulsion at a wide range of particle separations, particularly in the $|\gamma| > 1$ regimes. This phenomenon can be understood from the

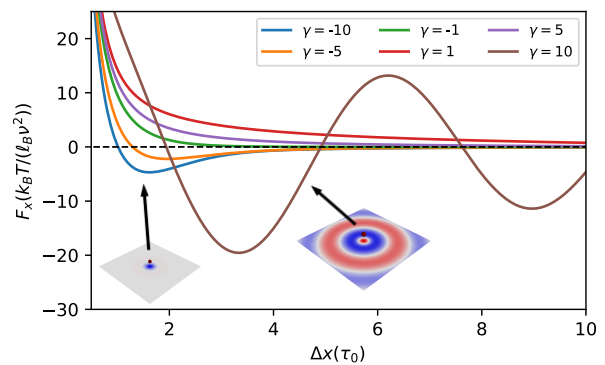


FIG. 2. Force between two particles with charge νe_0 in a quasi-2D system of size $(30\tau_0, 30\tau_0, 2\tau_0)$, and the medium's Bjerrum length $\ell_B = 3.5\tau_0$. Particles are placed at $(15\tau_0, 15\tau_0, \tau_0)$ and $(15\tau_0 + \Delta x, 15\tau_0, \tau_0)$. Subfigures show induced charge density $\sigma(\mathbf{r})$ on the bottom substrate when $\gamma = 10$ or $\gamma = -10$, where red/blue represents positive/negative charges, respectively. For the case $|\gamma| < 1$, we also validate our method with ICM, results can be found in supplementary information (SI) [29].

induced surface charge density profiles. Because of symmetry, in the insets of Fig. 2 we examine the induced charge density $\sigma(\mathbf{r})$ on the bottom substrate at $z = 0$ due to the presence of a single charged particle located at \mathbf{r}_1 ,

$$\sigma(\mathbf{r}) = \lim_{z \rightarrow 0^+} \left(\frac{\epsilon}{\epsilon'} - 1 \right) e_0 \nu \frac{\partial G(\mathbf{r}; \mathbf{r}_1)}{\partial z}. \quad (2)$$

The insets show that in the case $\gamma = -10$, a positively charged particle will induce a strong negative surface charge density surrounding it, which can overwhelm the Coulomb repulsion and give LCA; while in the case $\gamma = 10$, a non-trivial oscillatory σ profile arises, and we attribute this to the complicated multiple scattering of the polarization field between the confinement substrates, as was also illustrated from the ICM view-

point. Note that many studies have documented that likely charged nanoparticles can attract each other due to polarization, but attraction often occurs under either charge- or size-asymmetric settings [30–32]. Thus the LCA and oscillation phenomena reported here are both new, which may further influence the collective behavior of charged particles under dielectric confinement.

The key idea of our method in efficiently solving for the Green's function Eq. (1) is originated from Ewald-splitting, but tailored for quasi-2D systems. Instead of using a spherical symmetric Gaussian cloud, we decompose the Dirac $\delta(\cdot)$ in a *cylindrical symmetric* manner, i.e.,

$$\delta(\mathbf{r}) = \left[\delta(\mathbf{r}) - \frac{\alpha}{\pi} e^{-\alpha\rho^2} \delta(z) \right] + \frac{\alpha}{\pi} e^{-\alpha\rho^2} \delta(z), \quad (3)$$

with $\boldsymbol{\rho} = (x, y)$, $\rho = \sqrt{x^2 + y^2}$, and the choice of α will be determined by considerations of computational efficiency. Here we choose $\alpha = \sqrt{N}/(L_x L_y)$ similar to the standard 3D Ewald summation. Physically, Eq. (3) can be understood as screening the point charge only in the transverse directions, which is sufficient for quasi-2D systems. It also avoids the subtle situation of Gaussian charge cloud overlapping the substrates.

Based on the splitting strategy Eq. (3), the Green's function can be decomposed into short- and long-range components, i.e., $G := G_1 + G_2$ with

$$G_1(\mathbf{r}; \mathbf{r}') = - \sum_{\mathbf{m}} \int_0^\infty \frac{1}{2\pi\epsilon} g(\kappa, z; z') \times \left(1 - e^{-\frac{\kappa^2}{4\alpha}} \right) J_0(\kappa\bar{\rho}_m) \kappa d\kappa, \quad (4)$$

$$G_2(\mathbf{r}; \mathbf{r}') = - \sum_{\mathbf{k}} \frac{1}{L_x L_y \epsilon} g(k, z; z') e^{-\frac{k^2}{4\alpha}} e^{i\mathbf{k}\cdot\bar{\boldsymbol{\rho}}}, \quad (5)$$

where $\bar{\boldsymbol{\rho}} = \boldsymbol{\rho} - \boldsymbol{\rho}'$, $\mathbf{k} = (k_x, k_y) = (\frac{2\pi m_x}{L_x}, \frac{2\pi m_y}{L_y})$ and J_0 the 0-th order Bessel function. One can show that G_1 and G_2 shares the same coefficients $g(k, z; z')$, given by (See SI [29] for more detailed derivations)

$$g(k, z; z') = \frac{\Gamma_0(k)}{2k} \left[\Gamma_1 e^{k(z'+z-2L_z)} + \Gamma_2 e^{-k(z'+z)} + \Gamma_3 e^{-k|z'-z|} + \Gamma_4 e^{k(|z'-z|-2L_z)} \right], \text{ for } k > 0, \quad (6)$$

where $\Gamma_0(k) = 1/[(\epsilon - \epsilon')^2 e^{-2kL_z} - (\epsilon + \epsilon')^2]$, $\Gamma_1 = \Gamma_2 = (\epsilon^2 - \epsilon'^2)$, $\Gamma_3 = (\epsilon + \epsilon')^2$ and $\Gamma_4 = (\epsilon - \epsilon')^2$.

Eq. (6) diverges as $k \rightarrow 0$, the 0-th mode need to be treated carefully. Physically, it corresponds to proposing the proper FBC as $z \rightarrow \pm\infty$ so that the divergent image charge series (as depicted in Fig. 1) can be renormalized. For $k = 0$, it is understood that the electric field should be a function of z only, hence $\hat{E}_{k \rightarrow 0}(z \rightarrow +\infty)$ and $\hat{E}_{k \rightarrow 0}(z \rightarrow -\infty)$ are both constants so as to satisfy

Gauss's law. The divergence issue thus can be properly renormalized, which leads us to

$$g(k=0, z; z') = -\frac{|z - z'|}{2}. \quad (7)$$

Physically, Eq. (7) implies that for $k = 0$, confined source charge acts as a uniformly charged plate.

In N particle simulations, the long-range component G_2 can be efficiently computed, because 1) fast convergence due to the prefactor $e^{-\frac{k^2}{4\alpha}}$; and 2) unlike Ewald2D method [33–35] which scales as $\mathcal{O}(N^2)$ since its reciprocal part is not separable, here G_2 can be computed as fast as Ewald3D since it only involves exponential terms which is *separable*, e.g., $e^{i\mathbf{k}\cdot(\boldsymbol{\rho}_i - \boldsymbol{\rho}_j)} = e^{i\mathbf{k}\cdot\boldsymbol{\rho}_i} \cdot e^{-i\mathbf{k}\cdot\boldsymbol{\rho}_j}$. However, computing the short-range part G_1 is challenging, since $J_0(z)$ decays slowly ($\sim z^{-1}$ as $z \rightarrow \infty$) and is oscillatory. To avoid numerically evaluating G_1 directly, we introduce the Hankel transform \mathcal{F} , $\mathcal{F}[f(r)] = 2\pi \int_0^\infty f(r) J_0(2\pi\kappa r) r dr = g(\kappa)$, and its inverse transform $\mathcal{F}^{-1}[g(\kappa)] = 2\pi \int_0^\infty g(\kappa) J_0(2\pi\kappa r) \kappa d\kappa = f(r)$. Based on the useful fact that

$$\left\{ \frac{1}{\sqrt{a^2 + r^2}}, \frac{e^{-2\pi a \kappa}}{\kappa} \right\}$$

is a Hankel transform pair, we are able to extract the slowly decaying component of G_1 analytically,

$$G_1 = \sum_{\mathbf{m}} \sum_{i=1}^4 \int_0^\infty [A_i(\kappa) e^{-\frac{\kappa^2}{4\alpha}} + B_i(\kappa) e^{-2\kappa L_z}] e^{\kappa a_i(z, z')} \times J_0(\kappa |\boldsymbol{\rho} - \boldsymbol{\rho}'_{\mathbf{m}}|) d\kappa + C_i / \sqrt{a_i(z, z')^2 + \bar{\rho}_m^2}, \quad (8)$$

where a_i are index coefficients of four exponential terms same as Eq. (6) so that $a_i \in (-2L_z, 0)$; $A_i(\kappa)$, $B_i(\kappa)$ and C_i are other coefficients with detailed expressions given in SI [29]. Clearly, all integrands in Eq. (8) are now associated with an exponential decay prefactor, a recently developed Gauss quadrature scheme can be applied to achieve optimal spectral accuracy [36]. Furthermore, due to the short-range nature of G_1 , the computational cost can be reduced to $\mathcal{O}(N)$ in a simulation by combining with neighbor-list algorithms. Compared to existing Ewald3D-based methods [14, 15, 37], our approach is tailored for quasi-2D and thus do not need any artificial vacuum zones in z and correction terms. Compared to other grid-based methods [38, 39], our approach has its natural merit since we do not require numerical discretization and solving linear systems. Particularly, it overcomes the divergence issue for $|\gamma| > 1$, which allows us to investigate the less explored metamaterial confinement cases.

We examine a prototypical quasi-2D charged system, namely binary mixture of charged particles described by the primitive model. The system contains $N/2$ cations and $N/2$ anions, each particle with same diameter τ_0 and valence ± 1 and is thus overall charge neutral. Assume

i -th particle is located at \mathbf{r}_i and carries charge q_i , the Hamiltonian of the system reads

$$\mathcal{H} = \frac{1}{2} \sum_{i,j=1}^N 'q_i q_j G(\mathbf{r}_i, \mathbf{r}_j) + U_{\text{LJ}}, \quad (9)$$

where $\sum_{i,j}'$ indicates that when $i = j$, the singularity due to the self Coulomb interaction should be discarded, and U_{LJ} is the shift-truncated Lennard-Jones (LJ) potential energy modeling the excluded-volume interactions. The present model discards other interactions may be important in experimental realizations, but also offers the advantage of isolating the dielectric confinement effect. Systems with similar setup have been investigated recently in Refs. [21, 23, 24].

In all the Molecular Dynamics (MD) simulations performed, we fix $N = 100$ and box size $30\tau_0 \times 30\tau_0 \times 10\tau_0$, yielding a particle volume fraction of 5.8×10^{-3} . The Bjerrum length for the solvent medium is set to be $\ell_B = 3.5\tau_0$. Temporal integration is performed via the Velocity-Verlet algorithm provided by LAMMPS [40] and temperature is controlled via Anderson thermostat with stochastic collision frequency $\omega = 0.1$. To isolate electrostatic effect, the reduced temperature T_r is defined as $T_r = k_B T / U_{\text{coul}}$, where $U_{\text{coul}} = e_0^2 / (4\pi\epsilon\ell_B)$ and we maintain $\epsilon_{\text{LJ}} = k_B T$ for both particle-particle and particle-substrate interactions. Then, without loss of generality, we are able to investigate the impact of dielectric confinement by adjusting only two parameters (γ and T_r).

In the $|\gamma| \leq 1$ regime, extensive simulation works have been done recently [23, 24] and no SSB phenomenon has been found, i.e., the density distributions of cations $\rho_+(\mathbf{r})$ and anions $\rho_-(\mathbf{r})$ always maintain symmetries of the system, given by 1) *cross symmetry* in the confined space: $\rho_+(\mathbf{r}) = \rho_-(\mathbf{r})$, 2) *longitudinal symmetry*: $\rho_{\pm}(x, y, z) = \rho_{\pm}(x, y, L_z - z)$, and 3) *transverse symmetry*: $\rho_{\pm}(x, y, z) = \rho_{\pm}(x', y', z)$. Our simulations give symmetric results for $|\gamma| \leq 1$, consistent as previous investigations (details are documented in SI [29]). In the following discussions we will focus on the strongly polarizable cases of $|\gamma| > 1$, where SSB phenomena arise.

Fig. 3(a) documents the cation/anion density profiles in z with $\gamma = 10$ and reduced temperature $T_r = 0.1, 1$ and 10. It clearly shows, for the first time, SSB phenomena in such dielectric confined charged system, where both the cross and longitudinal symmetries are broken. The inset plot shows a snapshot configuration for $T_r = 1$ after equilibrium, cations and anions separate spontaneously and forming *charge-separated liquids* on the opposing substrates. We also observe the loss in symmetry varies continuous as a function of temperature, i.e., the mixing rate of cations and anions can be controlled via increasing T_r . Videos displaying the MD trajectories for the charge separating process are documented in SI.

To understand the spontaneous charge separation

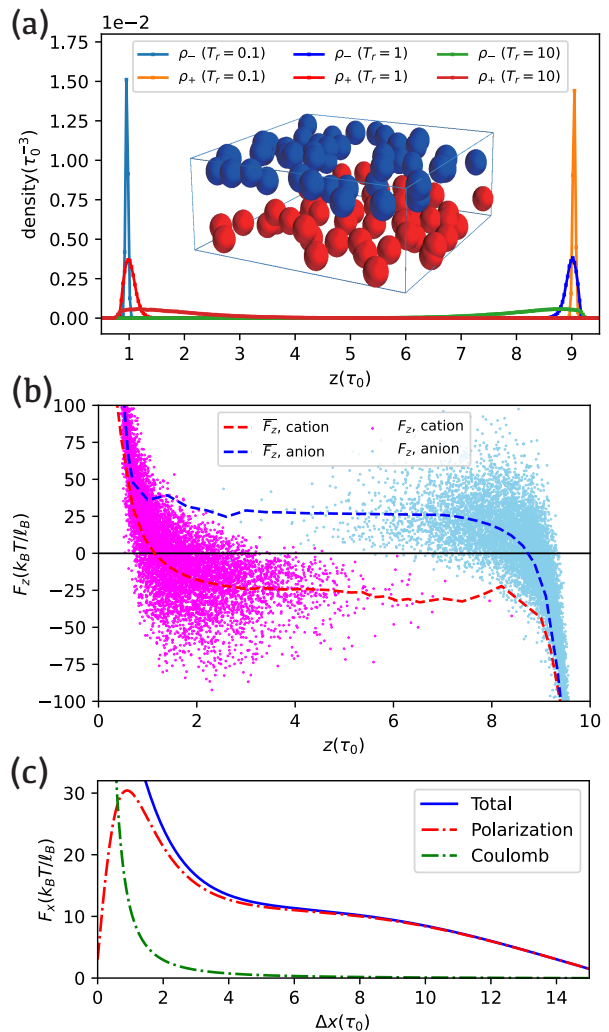


FIG. 3. Charge-separated interfacial liquids formation when $\gamma = 10$. (a) Ion density in z direction under different temperatures and inset for a typical equilibrium structure ($T_r = 1$) with red/blue particles represent cations/anions, respectively. (b) Force in z direction on cations and anions from 4000 independent snapshots when $T_r = 1$. Purple dots for cations and light blue for anions. Red and blue dashed lines are the potential of mean force \bar{F}_z acting on cation/anions. (c) Force in x direction between two cations on the interfacial liquid formation plane ($z \sim 0.64\tau_0$). Blue solid line represents the total force, while red dashed line for the polarization contribution and green dashed line for the bare Coulomb contribution.

mechanism, in Fig. 3(b) we plot the electrostatic force F_z exerts on each particle from 4000 independent snapshot configurations at $T_r = 1$ after equilibrium, where dashed lines indicate the potential of mean force \bar{F}_z . Clearly, \bar{F}_z is repulsive at short range but attractive if a particle leaves away from the substrate. The location $\bar{F}_z = 0$ also corresponds to the peak of density profiles in Fig. 3(a). Interestingly, though both substrates are overall neutral, they behave effectively as charged surfaces due to polar-

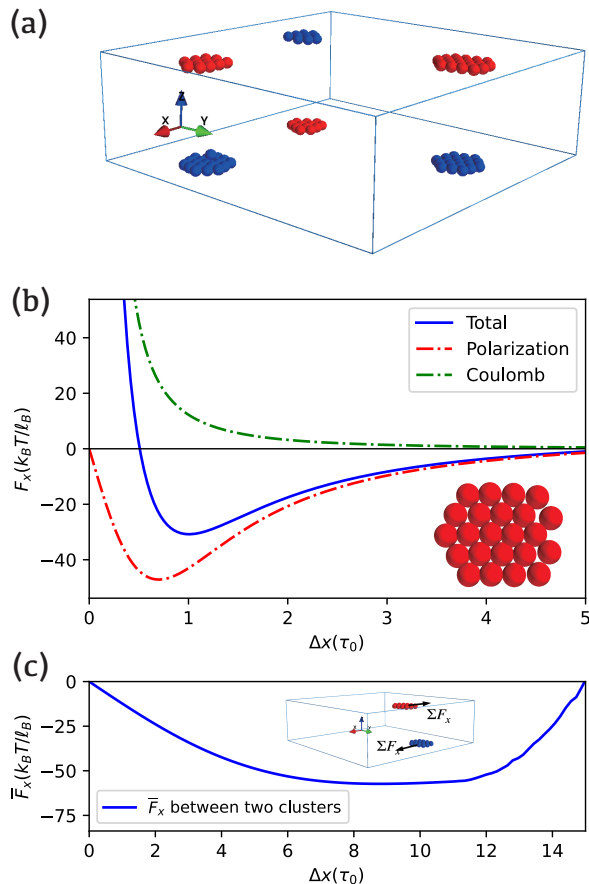


FIG. 4. Cluster formation when $\gamma = -10$. (a) Structure of equilibrium stats, red balls for cations, blue balls for anions. (b) Force in x direction for two cations on $z = 0.48\tau_0$ plane. The subfigure shows the structure of one cluster from (a). (c) Average force \bar{F}_x from one cluster to its partner, when there is a shift in x direction presented by Δx .

ization, and with *opposite* signs to the particles attached to them. This mechanism helps to stabilize the system.

To further understand why liquid phases are formed in transverse directions, in Fig. 3(c) we plot F_x between two cations as a function of separation Δx . The two cations are both placed at $z = 0.64\tau_0$, which is the interfacial liquid formation plane. Clearly, the cations are repulsive over the range $\Delta x \in [0, 15\tau_0]$, which is enhanced by dielectric confinement, leading to the formation of 2D liquids. Note that the oscillatory behavior observed in Fig. 2 still exists, but it occurs at long distance and is not strong enough to make an impact.

While the interfacial liquid phase breaks the longitudinal symmetry, the dielectric confined system can further break the transverse symmetry when $\gamma = -10$. Fig. 4(a) shows a typical snapshot configuration after equilibrium with $\gamma = -10$ and $T_r = 1$, where clusters are formed by likely-charged particles near the substrates (videos displaying the MD trajectories for the cluster formation

process are documented in SI). Each cluster is hexagonal close packed with gyration radius $R_g \sim 1.5\tau_0$, the top view of a typical cluster is shown in the inset of Fig. 4(b).

To understand the cluster formation mechanism, in Fig. 4(b) we examine F_x between two cations as a function of separation Δx with $z = 0.48\tau_0$, which is the cluster formation plane. Consistent with previous observation in Fig. 2, LCA arises over the range $\Delta x \in [0.5\tau_0, 5\tau_0]$, leading to the surprising cluster formation phenomenon for likely-charged particles.

Interestingly, we find that the clusters on opposing substrates are strongly correlated, i.e., there is a one-to-one “pairing” between the opposing clusters. In Fig. 4(c) we plot the average electrostatic force \bar{F}_x exerts on each cluster when two already paired clusters are shifted by a distance Δx from each other. Clearly, \bar{F}_x is always attractive, thus the clusters will be pulled back if shifted, forming stable opposing pairs. Experimentally, similar clustering phenomena have been reported for colloidal particles at air-water interfaces [41–43], but the phenomena reported here solely via dielectric confinement effect is clearly of different physical origin.

In summary, using a newly developed lattice summation method that permits simulations of dielectric confined quasi-2D charged systems, we are able to extensively explore the role of dielectric confinement effect. For a prototypical overall neutral charged system, it is discovered for the first time that spontaneous symmetry breaking can be induced and even modulated via the substrate polarizability alone. Our approach also provides a powerful tool for efficient and accurate simulation for a broad range of quasi-2D systems, with wide applications in future nanotechnology. Future plan includes further improve our method into an $\mathcal{O}(N)$ algorithm [44], and an open source implementation in LAMMPS [40].

Z. Gan acknowledges financial support from the National Science Foundation under Award No. CBET-1804940 and DMR-1420073. Z. Gan also wish to thank Aleksandar Donev and Leslie Greengard for helpful discussions on the physics and algorithms for quasi-2D charged systems.

* xz.gao@connect.ust.hk

† Corresponding author; zechenggan@ust.hk

- [1] M. Mazars, Long ranged interactions in computer simulations and for quasi-2D systems, *Phys. Rep.* **500**, 43 (2011).
- [2] R. Messina, Effect of image forces on polyelectrolyte adsorption at a charged surface, *Phys. Rev. E* **70**, 051802 (2004).
- [3] J. Yuan, H. S. Antila, and E. Luitjen, Structure of polyelectrolyte brushes on polarizable substrates, *Macromolecules* **53**, 2983 (2020).
- [4] M. Nishizawa, V. P. Menon, and C. R. Martin, Metal

- Nanotubule Membranes with Electrochemically Switchable Ion-Transport Selectivity, *Science* **268**, 700 (1995).
- [5] J. Cervera, B. Schiedt, R. Neumann, *et al.*, Ionic conduction, rectification, and selectivity in single conical nanopores, *J. Chem. Phys.* **124**, 104706 (2006).
- [6] Y. Levin, R. Pakter, and T. N. Teles, Collisionless relaxation in non-neutral plasmas, *Phys. Rev. Lett.* **100**, 040604 (2008).
- [7] M. Joyce and T. Worrakitpoonpon, Quasistationary states in the self-gravitating sheet model, *Phys. Rev. E* **84**, 011139 (2011).
- [8] R. Pakter and Y. Levin, Nonequilibrium Statistical Mechanics of Two-Dimensional Vortices, *Phys. Rev. Lett.* **121**, 020602 (2018).
- [9] E. Hückel and P. Debye, The theory of electrolytes: I. lowering of freezing point and related phenomena, *Phys. Z* **24**, 1 (1923).
- [10] V. G. Veselago, Electrodynamics of substances with simultaneously negative ϵ and ν , *Usp Fiziol Nauk* **92**, 517 (1967).
- [11] D. R. Smith, J. B. Pendry, and M. C. Wiltshire, Metamaterials and Negative Refractive Index, *Science* **305**, 788 (2004).
- [12] H. S. Antila and E. Luijten, Dielectric Modulation of Ion Transport near Interfaces, *Phys. Rev. Lett.* **120**, 135501 (2018).
- [13] Z. Wang and E. Luijten, Dielectric Modulation of Two-Dimensional Dipolar Materials, *Phys. Rev. Lett.* **123**, 096101 (2019).
- [14] A. Arnold, J. de Joannis, and C. Holm, Electrostatics in periodic slab geometries. I, *J. Chem. Phys.* **117**, 2496 (2002).
- [15] J. de Joannis, A. Arnold, and C. Holm, Electrostatics in periodic slab geometries. II, *J. Chem. Phys.* **117**, 2503 (2002).
- [16] S. Tyagi, A. Arnold, and C. Holm, ICMMM2D: An accurate method to include planar dielectric interfaces via image charge summation, *J. Chem. Phys.* **127**, 154723 (2007).
- [17] A. Fernández-Domínguez, S. Maier, and J. Pendry, Collection and Concentration of Light by Touching Spheres: A Transformation Optics Approach, *Phys. Rev. Lett.* **105**, 266807 (2010).
- [18] V. Jadhao, F. J. Solis, and M. O. De La Cruz, Simulation of Charged Systems in Heterogeneous Dielectric Media via a True Energy Functional, *Phys. Rev. Lett.* **109**, 223905 (2012).
- [19] J. W. Zwanikken and M. Olvera de La Cruz, Tunable soft structure in charged fluids confined by dielectric interfaces, *Proc. Natl. Acad. Sci. U.S.A.* **110**, 5301 (2013).
- [20] F. Fahrenberger and C. Holm, Computing the Coulomb interaction in inhomogeneous dielectric media via a local electrostatics lattice algorithm, *Phys. Rev. E* **90**, 063304 (2014).
- [21] A. P. Dos Santos, M. Girotto, and Y. Levin, Simulations of Coulomb systems confined by polarizable surfaces using periodic Green functions, *J. Chem. Phys.* **147**, 184105 (2017).
- [22] S. Yu and H. Ammari, Plasmonic Interaction between Nanospheres, *SIAM Rev.* **60**, 356 (2018).
- [23] J. Liang, J. Yuan, E. Luijten, and Z. Xu, Harmonic surface mapping algorithm for molecular dynamics simulations of particle systems with planar dielectric interfaces, *J. Chem. Phys.* **152**, 134109 (2020).
- [24] J. Yuan, H. S. Antila, and E. Luijten, Particle-Particle Particle-Mesh algorithm for electrolytes between charged dielectric interfaces, *J. Chem. Phys.* **154**, 094115 (2021).
- [25] O. Maxian, R. P. Peláez, L. Greengard, and A. Donev, A fast spectral method for electrostatics in doubly periodic slit channels, *J. Chem. Phys.* **154**, 204107 (2021).
- [26] W. G. McMillan Jr and J. E. Mayer, The Statistical Thermodynamics of Multicomponent Systems, *J. Chem. Phys.* **13**, 276 (1945).
- [27] Y. Urzhumov, W. Chen, C. Bingham, *et al.*, Magnetic levitation of metamaterial bodies enhanced with magnetostatic surface resonances, *Phys. Rev. B* **85**, 054430 (2012).
- [28] M. W. Coffey, Magnetic levitation from negative permeability materials, *Phys. Lett. A* **376**, 2739 (2012).
- [29] See Supplementary Information at [url] for detailed mathematical derivations, numerical quadrature scheme, its error analysis, and numerical validations, which includes refs. [23, 24, 36], .
- [30] E. Bichoutskaia, A. L. Boatwright, A. Khachatourian, and A. J. Stace, Electrostatic analysis of the interactions between charged particles of dielectric materials, *J. Chem. Phys.* **133**, 024105 (2010).
- [31] J. Lekner, Electrostatics of two charged conducting spheres, *Proc. R. Soc. A* **468**, 2829 (2012).
- [32] Z. Xu, Electrostatic interaction in the presence of dielectric interfaces and polarization-induced like-charge attraction, *Phys. Rev. E* **87**, 013307 (2013).
- [33] D. Parry, The electrostatic potential in the surface region of an ionic crystal, *Surf. Sci.* **49**, 433 (1975).
- [34] D. Heyes, M. Barber, and J. Clarke, Molecular dynamics computer simulation of surface properties of crystalline potassium chloride, *J. Chem. Soc., Faraday Trans. 2* **73**, 1485 (1977).
- [35] S. W. De Leeuw and J. W. Perram, Electrostatic lattice sums for semi-infinite lattices, *Mol. Phys.* **37**, 1313 (1979).
- [36] L. N. Trefethen, Exactness of Quadrature Formulas, *SIAM Rev.* **64**, 132 (2022).
- [37] I.-C. Yeh and M. L. Berkowitz, Ewald summation for systems with slab geometry, *J. Chem. Phys.* **111**, 3155 (1999).
- [38] A. Maggs and V. Rossetto, Local Simulation Algorithms for Coulomb Interactions, *Phys. Rev. Lett.* **88**, 196402 (2002).
- [39] D. Lindbo and A.-K. Tornberg, Fast and spectrally accurate Ewald summation for 2-periodic electrostatic systems, *J. Chem. Phys.* **136**, 164111 (2012).
- [40] A. P. Thompson, H. M. Aktulga, R. Berger, *et al.*, LAMMPS - a flexible simulation tool for particle-based materials modeling at the atomic, meso, and continuum scales, *Comp. Phys. Comm.* **271**, 108171 (2022).
- [41] G. Y. Onoda, Direct observation of two-dimensional, dynamic clustering and ordering with colloids, *Phys. Rev. Lett.* **55**, 226 (1985).
- [42] R. McGorty, J. Fung, D. Kaz, and V. N. Manoharan, Colloidal self-assembly at an interface, *Mater. Today* **13**, 34 (2010).
- [43] V. Lotito and T. Zambelli, Approaches to self-assembly of colloidal monolayers: A guide for nanotechnologists, *Adv. Colloid Interface Sci.* **246**, 217 (2017).
- [44] S. Jin, L. Li, Z. Xu, and Y. Zhao, A random batch Ewald method for particle systems with Coulomb interactions, *SIAM J. Sci. Comput.* **43**, B937 (2021).